JOURNAL OF MATERIALS SCIENCE 32 (1997) 5457–5465

An improved analysis for axisymmetric stress distributions in the single fibre pull-out test

M. Y. QUEK, C. Y. YUE
School of Mechanical and Production Engineering, Nanyang Technological University, Nanyang Avenue, Singapore 2263

Elastic stress transfer in the fibre pull-out problem has been investigated quite extensively using various shear lag analyses. These analyses grossly underestimate the severity of the stress concentration at the fibre–matrix interface. In this study, by using the total complementary energy approach, it is found that a stress concentration zone exists at the interface near the fibre entry. Compared to shear lag analysis, the interfacial radial stress at the fibre entry is found to be much higher and the interfacial shear stress reaches a maximum not at the entry end of the fibre but in a few fibre diameters from it. It is also shown that the magnitudes of these stress peaks reduce with increasing b/a and L/a ratios. At large b/a and L/a ratios, the maximum radial and shear stresses at the interface reach a plateau and are independent of the loading methods considered. Finally, the implications of these stress concentrations on the failure of the matrix and interface and the specimen geometry in determining the interfacial shear strength are discussed.

1. Introduction

1.1. Elastic stress transfer analysis

Elastic stress transfer is crucial to the understanding of interfacial debonding between the fibre and matrix in the fibre pull-out problem, idealized in Fig. 1. This is because the shear bond strength or interfacial shear strength between the fibre and the matrix is determined from a correlation of the experimental data and the stress distribution at the fibre–matrix interface derived from theory. To analyse the elastic stresses at the bonded surface between the fibre and matrix, various analytical and numerical models [1–5] have been developed. The assumptions common to these different approaches are that the fibre and matrix are considered to be isotropic, homogeneous and linear elastic and that the bonding between the fibre and matrix is perfect. At the interface between the fibre and matrix, there exists a very small volume of material known as the interphase layer. Because the properties of the interphase cannot be determined accurately, the interphase is assumed to have the same properties as the bulk matrix. Also, the transition from matrix to fibre is modelled as a sharp corner rather than a meniscus as this is regarded as having the most critical influence on the stress field.

Of the several models mentioned above, it is noted that the shear lag analysis grossly underestimates the severity of the stress concentration at the fibre entry. The magnitude of the interfacial radial stress at the fibre entry is predicted to be much less than the interfacial shear stress [1]. Finite element studies [5, 6] on the other hand, yield results that are the exact opposite. In the case of shear lag models, the radial strains in the matrix are often assumed to be negligible in comparison with the axial and shear strains. This assumption might account for the wide differences in radial stress distributions between shear lag and finite element analyses.

Another observation is that a maximum value of the interfacial shear stress, τ_i, is predicted at the entry end of the fibre. This does not, however, satisfy the traction-free boundary condition on the matrix surface perpendicular to the fibre entry in the physical problem and, is in violation of the principle of complementary shear stresses. For the fixed matrix bottom (FMB) loading method shown in Fig. 1a, in which only an axial stress is applied to the fibre, the surface of the matrix at the fibre entry is stress free. Thus, an element of the matrix, as shown in Fig. 1a, is in a state of plane stress. Apart from the surface of the matrix at the outer radius, $r = b$, surfaces elsewhere on which a plane state of stress exists are marked in Fig. 1.

The reason for this finite value of τ_i at the fibre entry is that there are more boundary conditions to be satisfied than required for solution of the stresses in the fibre [2]. The choice of which boundary conditions must be satisfied determines whether or not the solutions for the stresses in the fibre and matrix are reasonable and realistic. When the boundary conditions, including the stress free boundary condition on the surface of the matrix at the fibre entry are completely satisfied, as in the three-dimensional elasticity solution of the pull-out problem, maximum interfacial shear stress occurs not at the fibre entry but a few fibre diameters from it [4]. However, the methodology is more complex and numerical difficulties encountered in the solution process give rise to oscillatory

0022–2461

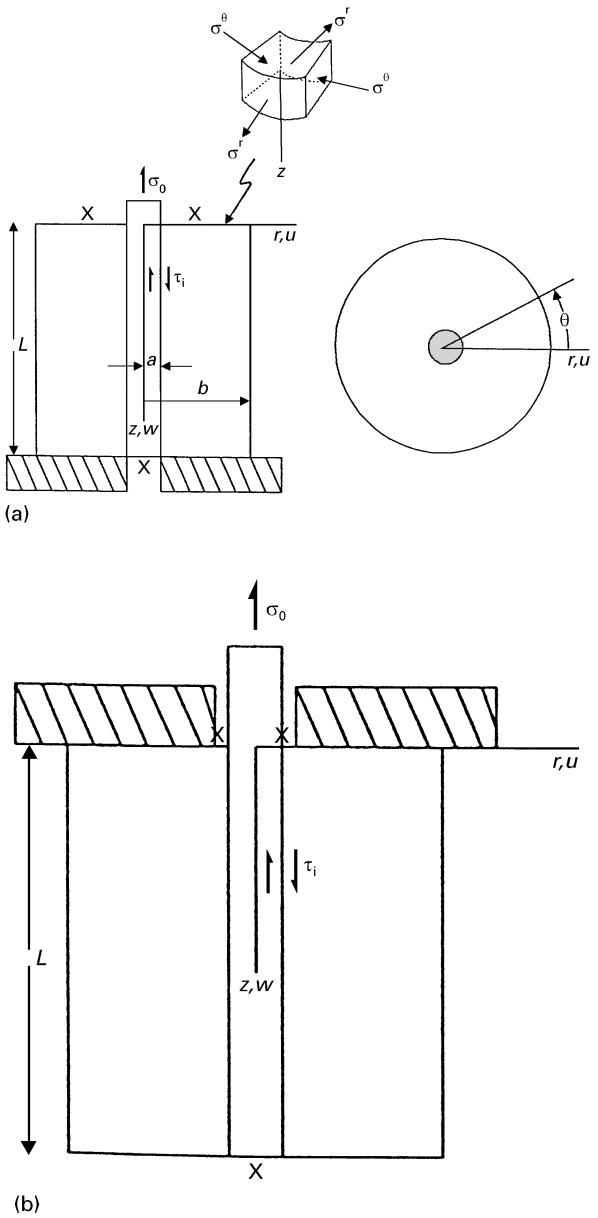

Figure 1 Schematic illustrations of loading methods on fibre pull-out for (a) fixed matrix bottom and (b) restrained matrix top. (X) Stress free surfaces.

behaviour of the radial stress fields in the stress concentration region near the fibre–matrix interface.

1.2. Stress singularity

In linear elasticity theory, it is recognized that singularities generally occur at the corners of geometric boundaries in which two dissimilar materials are joined together, such as at the square corner between the fibre and matrix at the entry end of the fibre. Finite element results seem to indicate the existence of such a singularity. However, to conclude that the stresses (in this case, the shear stress) are singular because they are large in magnitude is misleading because the stresses are extrapolated to the nodal points and as such, the stresses computed at a given point are essentially "smeared". Also, when the stress gradient is very steep over a very short distance, such as near the free surface corner between the fibre and matrix, it is doubtful whether the finite element method has adequate resolution to pick up the rapid change in the shear stress. Furthermore, it is noted that the finite element procedure does not allow stress free boundary conditions to be imposed in the solution process. Studies [7] have shown that at best, finite element results are known to be accurate only in a region very close to the stress concentration zone. More recently, finite elements results [8, 9] have shown that the interfacial shear stress reaches a maximum not at the fibre entry but within a very short distance from it and that the stress fields at the fibre entry are definitely not singular. Nevertheless, a stress concentration zone would be expected at the interface near the fibre entry.

The above discussions have intimated the possibility of zero interfacial shear stress at the fibre entry [10]. This notion seems plausible in spite of the lack of experimental data, if stress photoelastic "measurements" for fibre push-out [11] are accepted as indicative of similar stress distributions in the fibre pull-out problem.

1.3. An improved analysis

The discussions in the preceding sections highlight the shortcomings in the shear lag theory and the need for a more accurate analytical approach to determine the severe stress concentrations at the interface between the fibre and matrix at the fibre entry. The use of the total complementary energy principle is proposed. This principle has been applied recently to the study of the stress distributions in the fibre–matrix system [12]. Such a technique utilizes assumed stress functions that satisfy exactly the axisymmetric differential equations of equilibrium from the linear theory of elasticity. The assumed stress functions take into consideration the stress variations in both the radial as well as axial directions. The exact forms of these stress functions are found from the boundary conditions of the problem and by minimizing the total complementary energy in the fibre and matrix. An advantage of this technique is that as many energy terms as necessary can be included. However, the method becomes more complicated but is less complex in comparison with the three-dimensional elasticity solution [4]. In the following sections, an improved analysis is developed and used to determine the stress concentrations at the fibre–matrix interface.

2. Analytical procedure

The total complementary energy approach to the solution of axisymmetric stress distributions in a fibre embedded in a hollow cylindrical matrix is well documented [12]. The complementary strain energy in the linear elastic fibre–matrix system is given by

$$U = \iiint_v \frac{1}{2}\sigma_{ij}\varepsilon_{ij}\,dv \quad (i, j = 1, 2, 3)$$

$$= \iiint_v \left(\frac{1}{2}\sigma_{zz}\varepsilon_{zz} + \underline{\frac{1}{2}\sigma_{rr}\varepsilon_{rr}} + \underline{\frac{1}{2}\sigma_{\theta\theta}\varepsilon_{\theta\theta}} + \tau_{rz}\varepsilon_{rz} + \tau_{r\theta}\varepsilon_{r\theta} + \tau_{\theta z}\varepsilon_{\theta z}\right) dv \qquad (1)$$

Because the problem is axisymmetric, $\tau_{r\theta} = \tau_{\theta z} = 0$. In the previous analysis [12], the underlined terms, which are the complementary strain energy contributions due to the radial and circumferential stresses, were neglected. The minimization of U^* then resulted in a second-order differential equation requiring only two boundary conditions for its solution. The boundary conditions to be satisfied are the same as those employed in the shear lag analysis, namely, that $\sigma = \sigma_0$, the applied stress at the entry end of the fibre ($z = 0$) and $\sigma = 0$ at the exit end ($z = L$), in Fig. 1. However, as pointed out in [2], there are in fact more than two boundary conditions to be satisfied, the third condition being that the shear stress is zero along the matrix surface ($r \geqslant a, z = 0$) for the FMB loading condition. A fourth condition not mentioned in [2], arises at the interface between the fibre and matrix at the exit end of the fibre, $z = L$. Here, the stress free surface of the fibre dictates that the interfacial shear stress at the square corner between the fibre and matrix is also zero. Now, a judicious choice of which of the four boundary conditions are to be satisfied has to be made in order to obtain reasonable stress solutions. The final choice disregards the stress free boundary conditions and inevitably, leads to a finite value of τ_i at the entry end of the fibre [2]. This discrepancy can be corrected using the total complementary energy approach. By including the underlined terms in Equation 1, the resulting differential equation following the minimization process would be of fourth-order. All the four boundary conditions can now be utilized to obtain a more complete solution. However, the process becomes more tedious because the integrands in Equation 1 are more complicated. The details of the procedure are given in the Appendix.

3. Results and discussion

3.1. Comparison with a previous analysis

3.1.1. The fixed matrix bottom loading method

Results from the present analysis are compared with those from a previous analysis [12]. Fig. 2a–e shows the stress distributions normalized to the applied stress, σ_0, in a carbon fibre–epoxy composite for the FMB loading condition. The position of $z = 0$ corresponds to the fibre entry. The composite has the following properties: $E_f = 230$ GPa, $E_m = 3$ GPa, $\upsilon_f = 0.2$, $\upsilon_m = 0.4$, $b/a = 20$, $L = 0.5$ mm. A stress of $\sigma_0 = 1.0$ GPa is applied to the fibre. From Fig. 2a it is seen that the axial stress in the fibre is increased while the axial stress in the matrix, Fig. 2b, is correspondingly reduced. The turning point at $z = 0$ in Fig. 2a ensures stress continuity in the protruding length of the fibre where σ_0 is applied. The most significant differences observed are the shear stress, τ_i and the radial stress, σ_i^r, at the interface due to Poisson's effect. Fig. 2c shows two "humps" in the interfacial shear stress distribution along the fibre. The first maximum occurs near the entry end of the fibre and is much larger than the magnitude of the second maximum near the exit end. There is also a significant reduction in the maximum interfacial shear stress, $\tau_{i(max)}$, near the entry end of the fibre. $\tau_{i(max)}$ from the present analysis is only about 70% of the finite value from the previous analysis. This suggests that the interfacial shear strength, τ_s, determined from fibre pull-out test data using shear lag analysis would be a conservative estimate. Also, $\tau_{i(max)}$ occurs about five–six fibre diameters from the fibre entry end. In Fig. 2d, the maximum radial interfacial stress, $\sigma_{i(max)}^r$, at the fibre entry is about five–six times the value obtained previously and is much larger than $\tau_{i(max)}$. The interfacial radial stress, σ_i^r, decreases very rapidly along the fibre, changing from tensile to compressive in a few fibre diameters from the fibre entry. At fibre entry in the radial direction, there is a more gradual decrease in the radial stress distribution $\sigma_m^r(r \geqslant a, z = 0)$, in the matrix as shown in Fig. 2e. The interfacial circumferential stress in the matrix σ_m^θ, is of the same magnitude as σ_m^r but is compressive.

From this improved analysis, it may be stated that at the fibre entry, the fibre–matrix interface is subjected to a severe stress concentration due to the very large radial and circumferential stresses. A few fibre diameters away, the interfacial shear stress, τ_i, reaches a maximum. Note that a material point of the matrix at the free surface is in a state of plane stress (Fig. 1), with $\sigma_{m(max)}^r$ (tensile) and $\sigma_{m(max)}^\theta$ (compressive) being the principal stresses. The maximum shear stress in the element has the same magnitude and acts on planes inclined at 45° to the $r - \theta$ direction. The effects of these stress concentrations on debonding between the fibre and matrix and on the failure of the matrix will be discussed in a later section.

3.1.2. Restrained matrix top (RMT) loading method

Fig. 3a–e shows the stress distributions in the same fibre–matrix system with the matrix top restrained. The results are similar to FMB, with $\tau_{i(max)}$ significantly reduced and $\sigma_{i(max)}^r$ very large at the entry end of the fibre compared with the previous analysis. $\tau_{i(max)}$ and $\sigma_{i(max)}^r$ for the RMT loading method are greater than for FMB, agreeing with previous analysis [1, 12]. It is noted that an element of the matrix beneath the top restraint is in a three-dimensional state of stress.

3.2. The influence of radial stresses on failure in the pull-out test

The severe stress concentration near the fibre entry will cause failure of the fibre–matrix interface. The mode of failure will depend on the relative magnitudes of the interfacial radial and shear stresses. Specimen geometry, defined in terms of the b/a and L/a ratios, is anticipated to have an influence on their relative magnitudes and will now be considered.

3.2.1. Influence of b/a *ratio*

The influence of the b/a ratio on the stress distributions in the fibre–matrix composite is investigated. The results for four values of b/a ratios are shown in

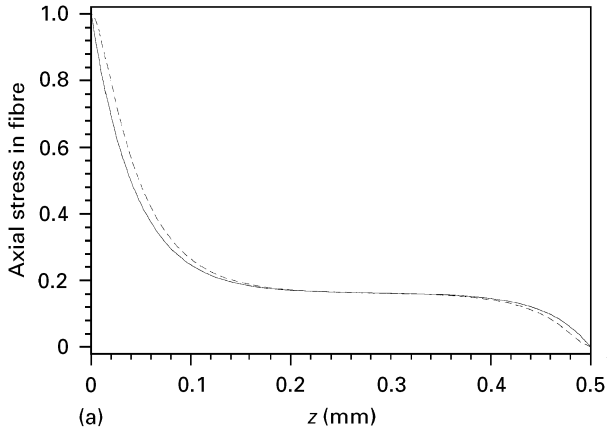

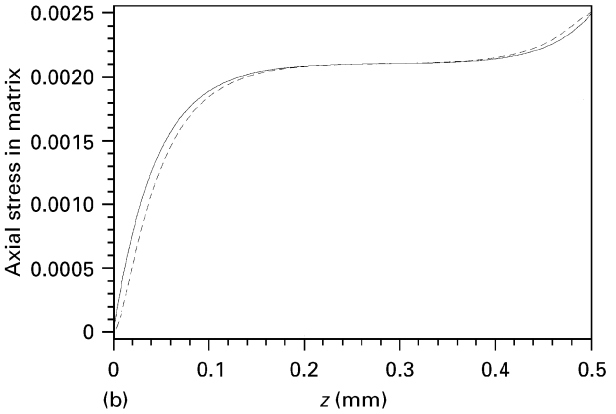

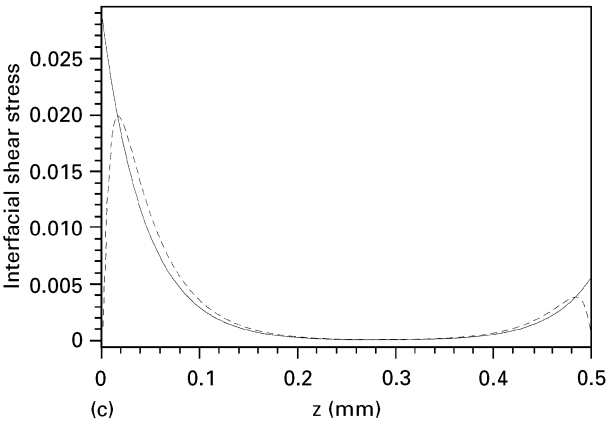

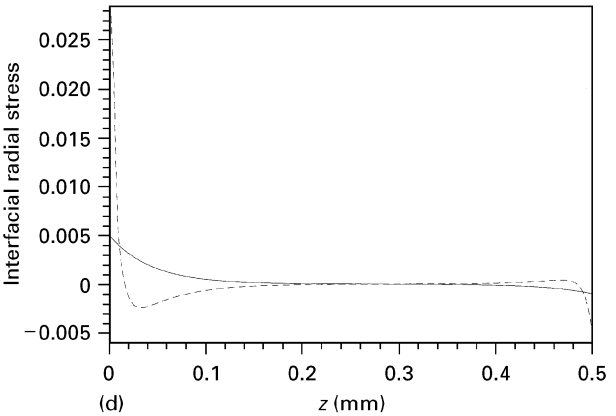

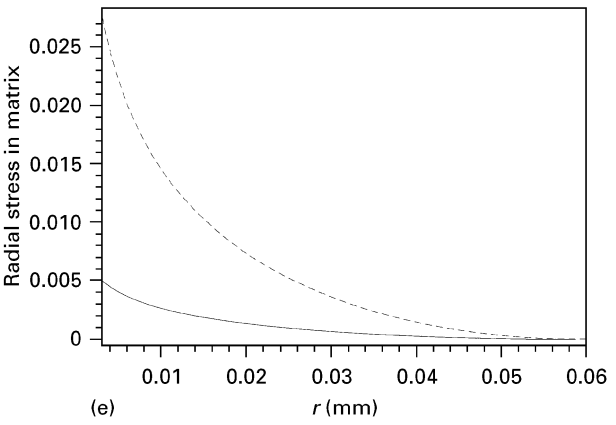

Figure 2 Comparison of normalized stress distributions in the FMB loading configuration between present analysis (– – – –) and previous analysis (——). (a) axial fibre stress, (b) axial matrix stress, (c) interfacial shear stress, (d) interfacial radial stress, along the z-direction; and (e) radial stress in the matrix in the direction of thickness.

Fig. 4a–d for FMB and Fig. 5a–d for RMT loading methods.

At a ratio of $b/a > 90$, the stress distributions in the fibre for both loading methods have become quite identical (Figs 4a and 5a). Note the very rapid decrease in the axial stress in Fig. 4a at large b/a ratios. The shear stress transfer is spread over a longer distance at the interface resulting in lower peak stresses in comparison with the spikes at a smaller b/a ratio (Figs 4c and 5c). For the FMB loading method, the first maximum of τ_i near the entry end of the fibre is reduced, more slowly initially and then more rapidly, as the b/a ratio increases and the second maximum at the exit end of the fibre has almost completely disappeared when $b/a > 50$. In contrast, for the RMT loading method, the maximum interfacial shear stress drops sharply with an increase in b/a. A large b/a ratio also reduces the maximum interfacial radial stress, $\sigma^r_{i(max)}$, drastically (Figs 4d and 5d). For the FMB loading method, the radial stress at the interface at the fibre entry is tensile due to Poisson's contraction of the fibre, while at the exit end it is compressive due to Poisson's contraction of the matrix. At a small b/a ratio, σ^r_i for the FMB loading method at both the entry and exit ends of the fibre are nearly equal in magnitude. Fig. 6 elucidates the differences in the maximum stresses in the two loading methods as the b/a ratio is increased. At a small b/a ratio, the difference in the magnitudes of both the peak stresses, $\tau^r_{i(max)}$ and $\sigma^r_{i(max)}$, is more pronounced. The peak stresses for the RMT loading condition are greater than the corresponding stresses for the FMB loading condition at the same b/a ratio. For $b/a > 100$, $\tau^r_{i(max)}$ and $\sigma^r_{i(max)}$ for both loading methods are identical, with $\tau^r_{i(max)}$ greater than $\sigma^r_{i(max)}$. Beyond $b/a = 100$, the stresses reach a plateau indicating the independence of the maximum stresses upon the loading method.

From this study, it may be seen that at a large b/a ratio, the stress transfer is more effective in that the peak stresses are significantly reduced although this is accompanied by an increase in the axial stress in the fibre. It is easier to initiate debonding between the fibre and matrix at a small b/a ratio due to high interfacial radial stresses. A large b/a ratio should give a more consistent estimate of the interfacial shear

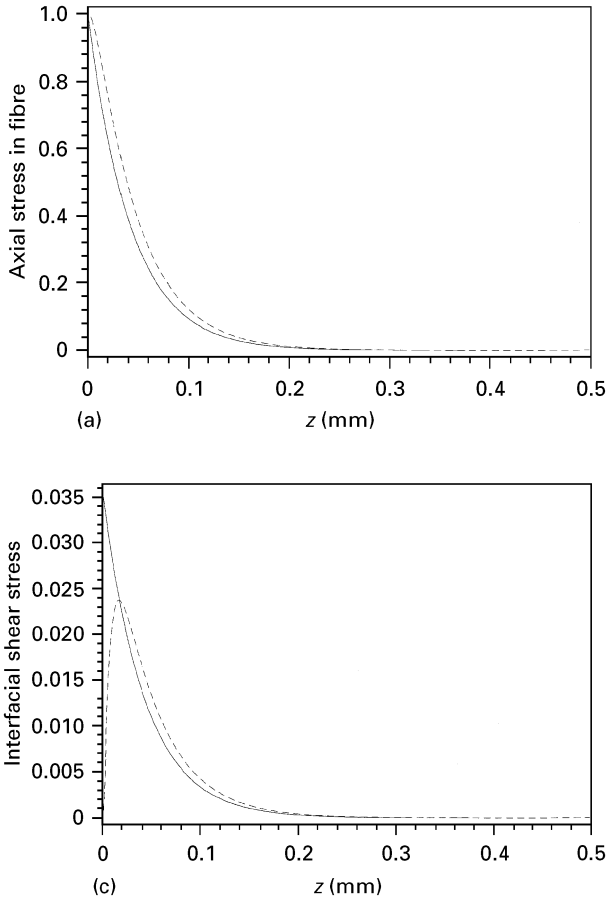

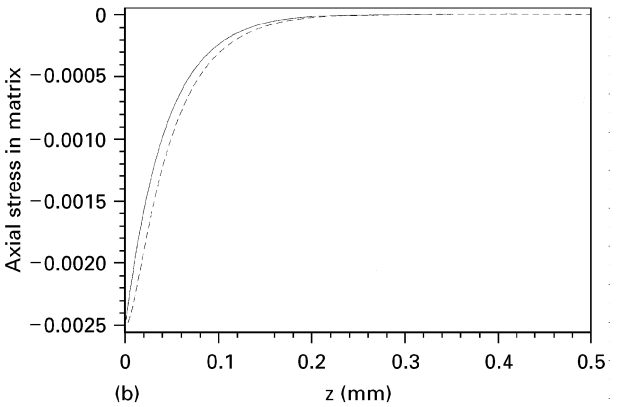

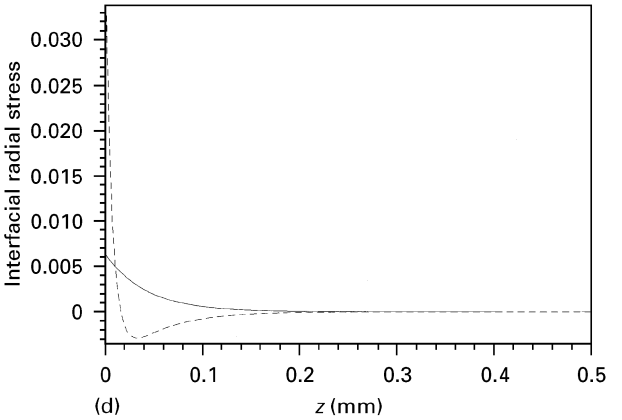

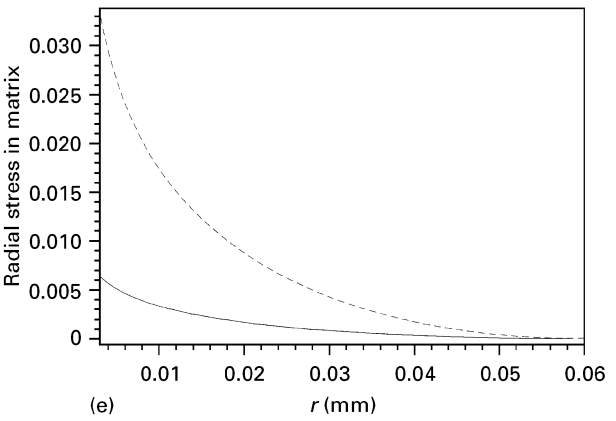

Figure 3 Comparison of normalized stress distributions in RMT loading configuration between present analysis (– – – –) and previous analysis (——): (a) axial fibre stress, (b) axial matrix stress, (c) interfacial shear stress, (d) interfacial radial stress, along the z-direction; and (e) radial stress in the matrix in the thickness direction.

strength, τ_s, using either the FMB or RMT loading method. Also to be considered important is the large reduction in the radial stress at the interface at large b/a ratios, which is likely to affect the initial mode of failure of the composite.

3.2.2. Influence of L/a ratio

It is known that interfacial debonding is unstable when very short fibres are used in the pull-out test. To investigate the cause of this instability, it is necessary to evaluate the effect of fibre length on the magnitude of the stresses at the interface. The results of such a study are shown in Fig. 7 where the normalized maximum radial and shear stresses at the interface are plotted against the L/a ratio. Both $\sigma^r_{i(max)}$ and $\tau_{i(max)}$ decrease in magnitude as the L/a ratio increases. The decrease in $\sigma^r_{i(max)}$ is very steep. At fibre lengths much less than $20a$, $\sigma^r_{i(max)}$ is much higher than $\tau_{i(max)}$. For $L/a > 100$, the magnitude of $\tau_{i(max)}$ is about twice that of $\sigma^r_{i(max)}$.

The reason for unstable interfacial debonding at very short fibre lengths becomes clear. It is caused by the combined effects of very large interfacial radial and shear stresses. On the other hand, at large L/a ratios, much reduced interfacial stresses allow for stable debonding.

3.2.3. Failure modes

The preceding analysis shows that there is a stress concentration in a very small zone at the interface near the fibre entry. The magnitude of the peak stresses is influenced by both the b/a and L/a ratios; decreasing with increasing b/a and L/a ratios. The interfacial radial stress is tensile and is a maximum at the entry end of the fibre, whereas τ_i is a maximum at a short distance into the fibre.

The state of stress near the interface is complicated by the presence of shrinkage stresses due to processing and subsequent cooling down to room temperature. These stresses are compressive and arise from the differences in the coefficients of thermal expansion and material properties of the fibre and matrix. The resultant radial stress at the interface is affected by the

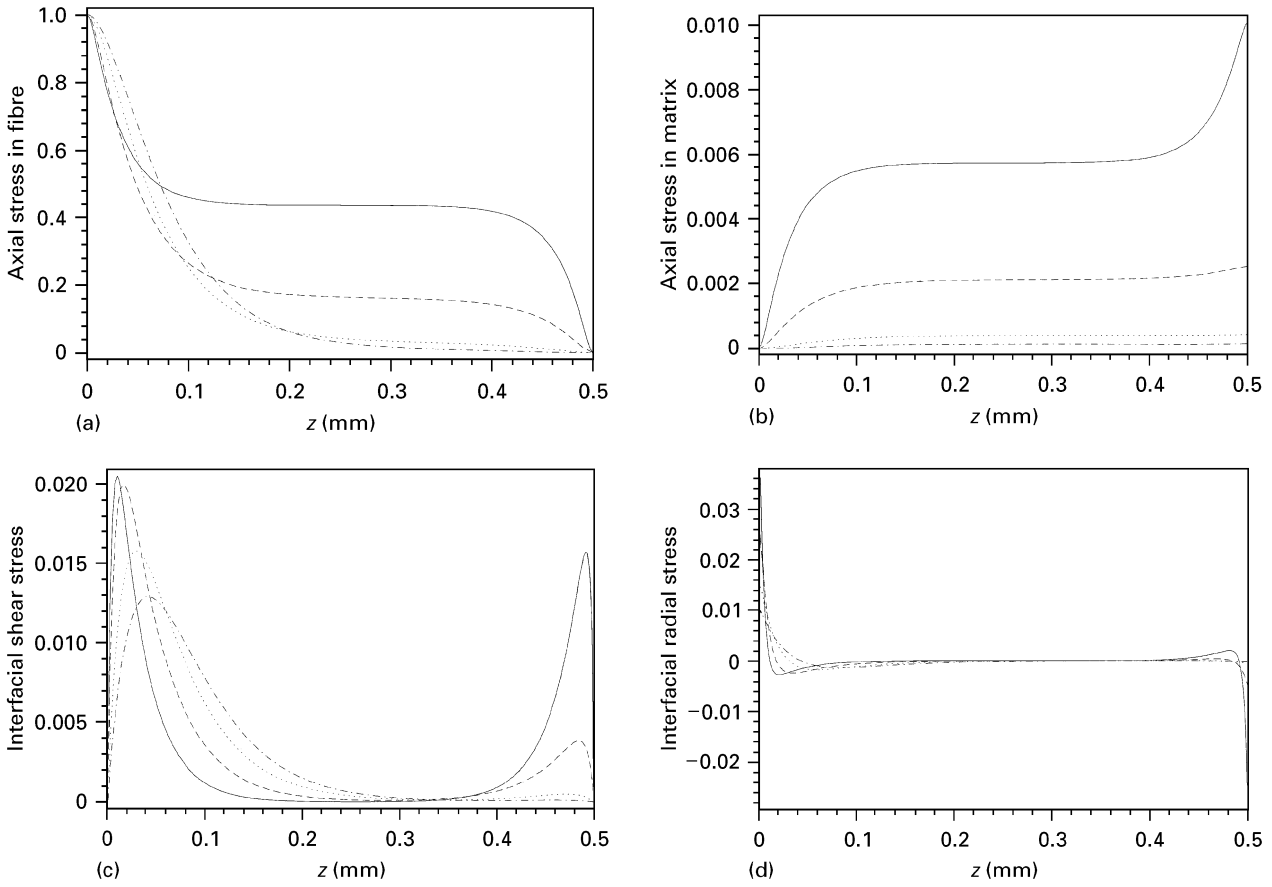

Figure 4 Influence of the b/a ratio on normalized stress distributions in the FMB loading configuration: (a) axial fibre stress, (b) axial matrix stress, (c) interfacial shear stress, and (d) interfacial radial stress, along the z-direction. (——) $b/a = 10$, (– – –) $b/a = 20$, (· · ·) $b/a = 50$, (–·–·) $b/a = 90$.

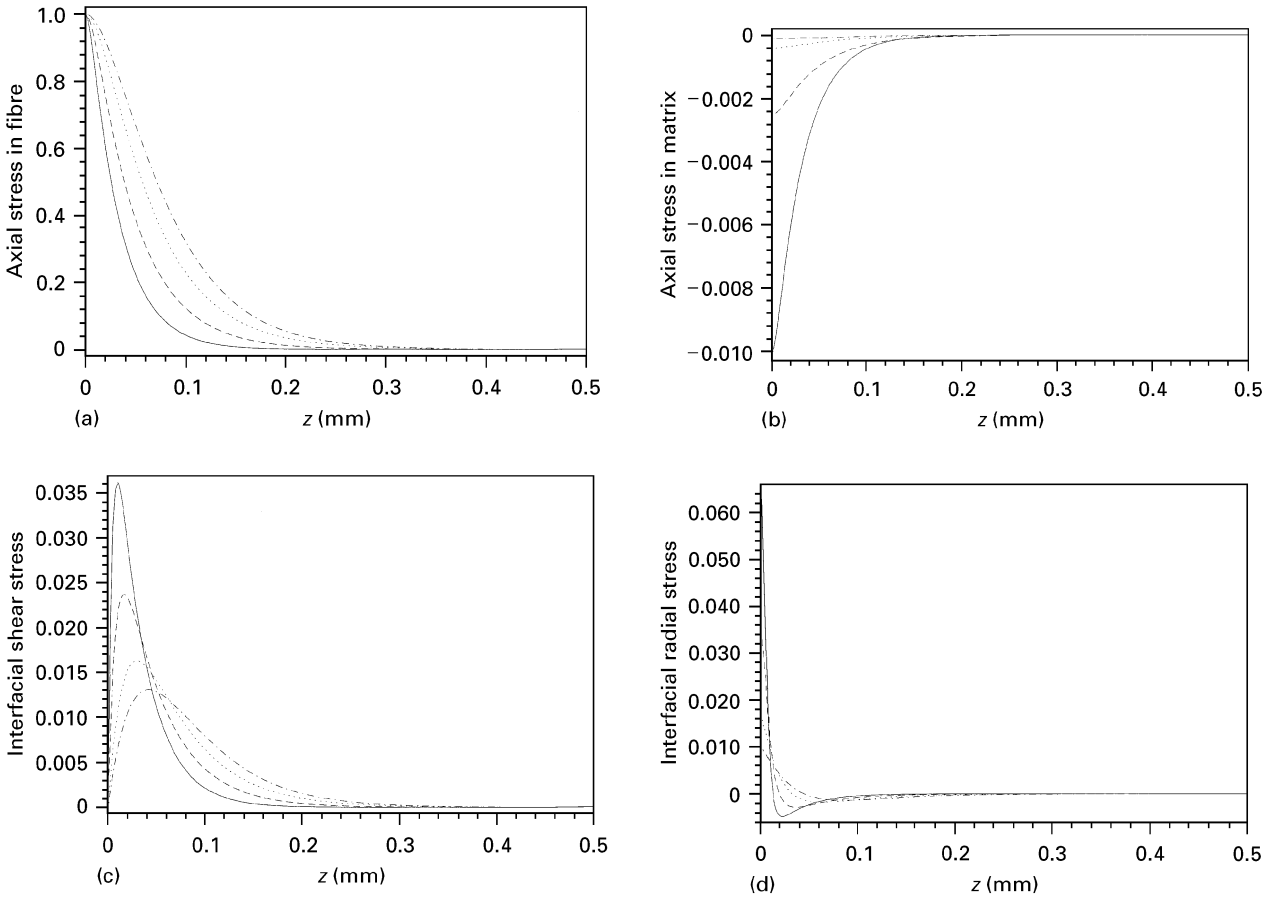

Figure 5 Influence of the b/a ratio on normalized stress distributions in the RMT loading configuration: (a) axial fibre stress, (b) axial matrix stress, (c) interfacial shear stress, and (d) interfacial radial stress, along the z-direction. (——) $b/a = 10$, (– – –) $b/a = 20$, (· · ·) $b/a = 50$, (–·–) $b/a = 90$.

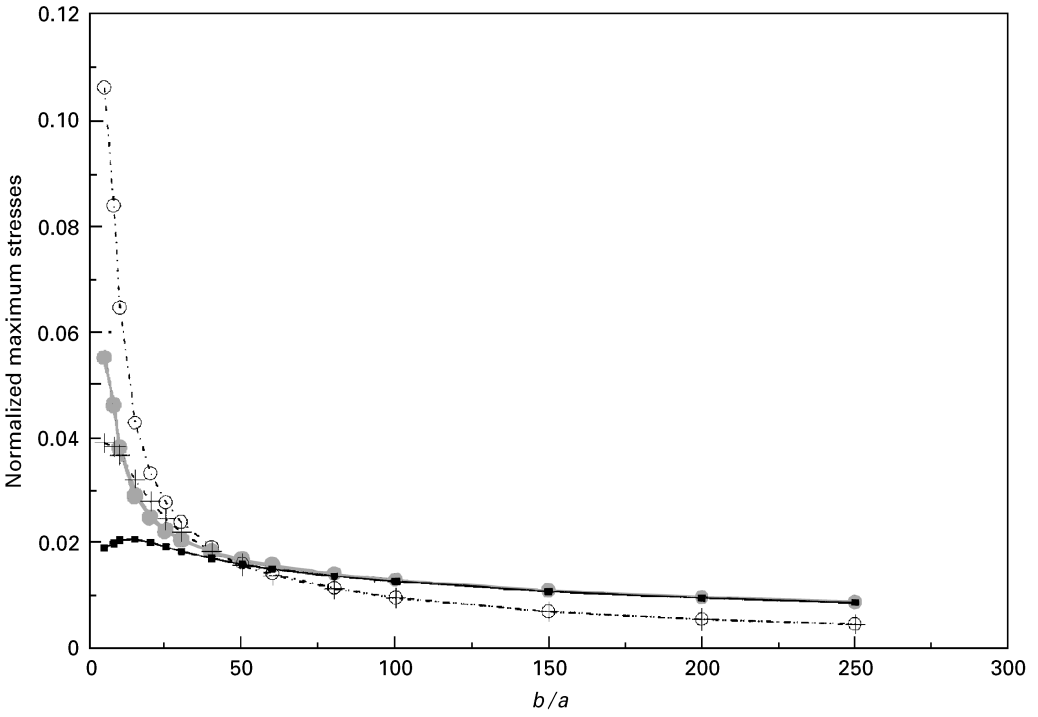

Figure 6 Comparison of the maximum normalized radial stress and shear stress at the interface for the RMT (⊖), (—●—) and FMB (· + ·), (—■—) loading methods, respectively, for different b/a ratios.

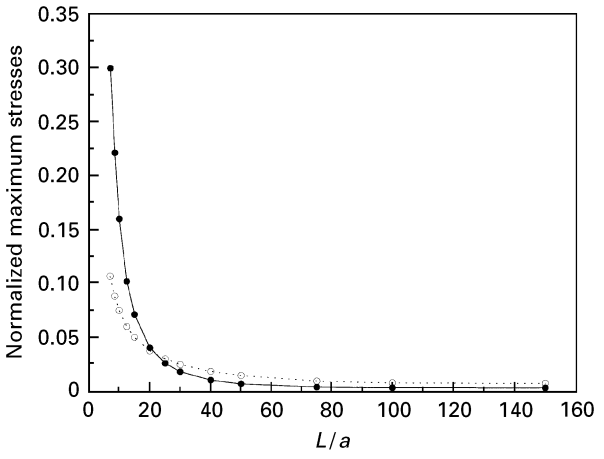

Figure 7 Effect of L/a ratio on the normalized maximum interfacial radial (—●—) and shear stresses (⊖) for the FMB loading method.

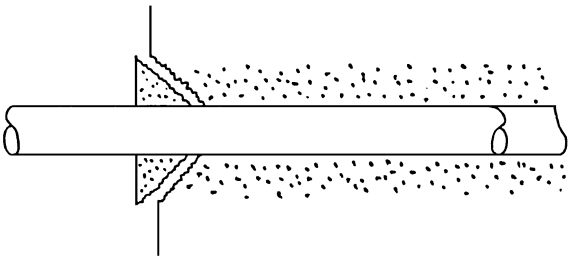

Figure 8 Matrix lump adhering to fibre end.

relative magnitudes of the shrinkage stress, and the maximum tensile interfacial radial stress, $\sigma^r_{i(max)}$, due to the Poisson's effect. For debonding due to the opening mode, the shrinkage stress must be overcomed by $\sigma^r_{i(max)}$. At small b/a ratios, $\sigma^r_{i(max)}$ is large and debonding is mode I dominant. As $\sigma^r_{i(max)}$ decreases with increasing b/a ratio, debonding based on the interfacial shear strength criterion becomes mode II dominant. At intermediate values of b/a, debonding is a mixed mode failure. With short fibre lengths, debonding becomes unstable due to the adverse combined effects of large interfacial radial and shear stresses. This further suggests that the mode of failure is highly dependent upon specimen geometry. Because debonding failure at small b/a and L/a ratios is mode I dominant, the use of such specimens to determine the interfacial shear strength would lead to erroneous results.

Apart from debonding, there is also the possibility of shear failure in the matrix. It has been observed [13, 14] that pulled-out fibres usually have a lump of matrix, roughly conical in shape, adhering to the fibres at the entry ends with debonding initiated at a very short distance from it. This phenomenon, as illustrated in Fig. 8, suggests that the matrix first fails in a "ring" around the fibre. From experimental observations, this shearing of the matrix does not initiate at the interface but at a very short distance from it. Yielding of the matrix appears to be constrained by the presence of the fibre. Also, the properties of the interface are different from those of the bulk matrix. Close to the interface, however, both the radial and circumferential stresses in the matrix are still very large (Figs 2e and 3e). It is not known, however, how the shrinkage stresses are distributed in the radial direction. Ignoring these for the moment, an explanation is offered for the shearing phenomenon in the matrix. The surface of the matrix perpendicular to the fibre entry end is in a state of plane stress. The

maximum shear stress, τ_{max}, is equal in magnitude to $\sigma^r_{m\,(max)}$ and acts on planes inclined at 45° to the r–θ direction. Thus, the matrix will fail in shear if τ_{max} equals the yield stress of the matrix. Because of inhomogeneity, yielding is likely to occur at weak spots in the matrix. The probability of shear failure in the matrix is higher at a small b/a ratio because the radial and circumferential stresses in the matrix are much higher resulting in a higher τ_{max} than at a larger b/a ratio.

The above discussion reveals that at the stress concentration zone near the interface, there is competition between failure initiation by debonding or matrix failure due to shear. Matrix failure is more likely to precede debonding at a smaller b/a ratio because the radial and circumferential stresses and hence τ_{max}, are increased (Fig. 6). Debonding at the interface is promoted for $b/a > 100$ because the magnitudes of the radial and circumferential stresses are less than τ_i.

4. Conclusions

An analytical method that is an improvement over the shear lag models in determining the elastic stress transfer in a perfectly bonded, linear elastic fibre–matrix system, is presented. This method is an extension of the total complementary energy approach developed previously and includes in its formulation, the complementary strain energies in the fibre and matrix due to radial and circumferential stresses. This method leads to complete satisfaction of the boundary conditions at the fibre ends and yields an axisymmetric stress solution is the fibre–matrix system that is more representative of the physical problem. The severity of the stress concentration due to the radial stresses at the interface is demonstrated. The interfacial shear stress is found to reach its maximum value in a few fibre diameters from the entry end of the fibre, while the interfacial radial stress at the fibre entry is predicted to be significantly higher than given in a previous analysis.

An increase in the b/a ratio causes shear stress transfer to take place over a longer distance at the interface, thereby reducing the peak stresses. The effect of these reductions is to alter the mode of debonding from being mode I dominant at a smaller b/a ratio to mode II dominant at a larger b/a ratio. Furthermore, at a small b/a ratio, yielding of the matrix at the free surface is more likely due to the high shearing stress caused by the stress concentration arising from the radial and circumferential stresses. Whereas, a large b/a ratio tends to promote debonding without the matrix yielding. When fibre lengths are very short, interfacial debonding becomes unstable due to the adverse combination of large radial and shear stresses at the interface near the fibre entry. Thus, the use of specimens with small b/a and L/a ratios in a fibre pull-out test to determine the interfacial shear strength should be avoided.

Appendix

An improved method for obtaining the stress distributions in the fibre and matrix has been developed. The technique is illustrated for the FMB loading condition. The details and definitions of symbols used are given in reference [10].

For FMB, the stresses are [10], for the fibre

$$\sigma_f^z = \sigma_0 g_1(z)$$

$$\tau_f^{rz} = -\frac{\sigma_0 r}{2}\frac{dg_1}{dz} \tag{A1}$$

$$\sigma_f^r = \sigma_f^\theta = \frac{\sigma_0}{4}\left[r^2 - \frac{2a^2k^2\ln(k)}{k^2-1}\right]\frac{d^2g_1}{dz^2}$$

and for the matrix

$$\sigma_m^z = \frac{\sigma_0}{k^2-1}[1 - g_1(z)]$$

$$\tau_m^{rz} = -\frac{\sigma_0}{2(k^2-1)}\left(-r + \frac{b^2}{r}\right)\frac{dg_1}{dz} \tag{A2}$$

$$\sigma_m^r = \sigma_m^\theta = \frac{\sigma_0}{4(k^2-1)}\left[b^2 - r^2 + 2b^2\ln\left(\frac{r}{b}\right)\right]\frac{d^2g_1}{dz^2}$$

where the subscripts f and m refer to the fibre and matrix respectively. r, θ and z are the cylindrical coordinates as shown in Fig. 1.

The generalized Hooke's law is

$$\varepsilon_z = \frac{1}{E}[\sigma_z - \upsilon(\sigma_r + \sigma_\theta)]$$

$$\varepsilon_\theta = \frac{1}{E}[\sigma_\theta - \upsilon(\sigma_z + \sigma_r)] \tag{A3}$$

$$\varepsilon_r = \frac{1}{E}[\sigma_r - \upsilon(\sigma_z + \sigma_\theta)]$$

Neglecting τ_f^{rz}, the complementary strain energy U^* in the fibre and matrix is, from Equation 1

$$U = 2\pi\iint\left(\frac{1}{2}\sigma_f^z\varepsilon_f^z + \frac{1}{2}\sigma_f^r\varepsilon_f^r + \frac{1}{2}\sigma_f^\theta\varepsilon_f^\theta + \frac{1}{2}\sigma_m^z\varepsilon_m^z + \frac{1}{2}\sigma_m^r\varepsilon_m^r + \frac{1}{2}\sigma_m^\theta\varepsilon_m^\theta + \tau_m^{rz}\varepsilon_m^{rz}\right)r\,dr\,dz \tag{A4}$$

Using Equation A3 in Equation A4 and noting that $\sigma^r = \sigma^\theta$, gives

$$U = 2\pi\iint\left[\frac{1}{2E_f}(\sigma_f^z)^2 + \frac{(1-\upsilon_f)}{E_f}(\sigma_f^r)^2 - 2\frac{\upsilon_f}{E_f}\sigma_f^z\sigma_f^r + \frac{1}{2E_m}(\sigma_m^z)^2 + \frac{(1-\upsilon_m)}{E_m}(\sigma_m^r)^2 - 2\frac{\upsilon_m}{E_m}\sigma_m^z\sigma_m^r + \frac{(1-\upsilon_m)}{E_m}(\tau_m^{rz})^2\right]r\,dr\,dz \tag{A5}$$

Each of the integrands in Equation A5 can be evaluated using the results from Equation A1. The simplified form of Equation A5, in which σ^r and σ^θ are neglected, has been considered previously [10]. Evaluation of the remaining terms is more difficult and the

following results are quoted.

$$\frac{(1-\upsilon_f)}{E_f}\int_0^L\int_0^a(\sigma_f^r)^2 r\,dr\,dz=\frac{\sigma_0^2a^6(1-\upsilon_f)}{96E_f}$$
$$\times\left\{1-\frac{6k^2\ln(k)}{k^2-1}+12\left[\frac{k^2\ln(k)}{k^2-1}\right]^2\right\}\int_0^L(g_1'')^2\,dz$$
$$\frac{(1-\upsilon_m)}{E_m}\int_0^L\int_a^b(\sigma_m^r)^2\,r\,dr\,dz=\frac{\sigma_0^2a^6(1-\upsilon_m)}{192(k^2-1)^2E_m}$$
$$\times[5k^6-6k^4-24k^4\ln(k)^2-12k^2\ln(k)+3k^2-2]$$
$$\times\int_0^L(g_1'')^2\,dz$$
$$-2\int_0^L\int_0^a\frac{\upsilon_f}{E_f}\sigma_f^z\sigma_f^r r\,dr\,dz=\frac{\upsilon_f}{8E_f}\sigma_0^2a^4$$
$$\times\left[\frac{4k^2\ln(k)}{k^2-1}-1\right]\int_0^L g_1g_1''\,dz$$
$$-2\int_0^L\int_a^b\frac{\upsilon_m}{E_m}\sigma_m^z\sigma_m^r r\,dr\,dz=\frac{\upsilon_m}{8E_m}\frac{\sigma_0^2a^4}{(k^2-1)}$$
$$\times[k^4-4k^2\ln(k)-1]\int_0^L(1-g_1)g_1''\,dz \qquad (A6)$$

where g_1 and $g_1''(d^2g_1/dz^2)$ are functions of z. Because $b\gg a$, $k^2-1\approx k^2$, and the above expressions may be further simplified. When these simplified expressions are substituted into Equation A5, it is seen that

$$U=2\pi\int_0^L F(g_1,g_1',g_1'')\,dz \qquad (A7)$$

The function g_1 that extremizes the complementary energy functional, U^*, is the extremal function that satisfies the Euler–Lagrange equation

$$-\frac{d^2}{dz^2}\left(\frac{\partial F}{\partial g_1''}\right)+\frac{d}{dz}\left(\frac{\partial F}{\partial g_1'}\right)-\frac{\partial F}{\partial g_1}=0 \qquad (A8)$$

subject to the following boundary conditions

$$g_1(z=0)=1,\quad g_1(z=L)=0,$$
$$g_1'(z=0)=0,\quad g_1'(z=L)=0 \qquad (A9)$$

From Equation A2, it may be deduced that the last two conditions are necessary because $\tau_m^{rz}(r\geqslant a,z=0)=\tau_m^{rz}(r\geqslant a,\ z=L)=0$ due to the stress free conditions on the surfaces of the matrix at the entry and exit ends of the fibre.

Substituting for F from Equation A7 into Equation A8 and performing the differentiations, results in a fourth-order linear differential equation in g_1 of thefollowing form

$$a_0g_1^{VI}+a_1g_1''+a_2g_1+C_0=0 \qquad (A10)$$

where

$$a_0=-k^2a^4\{2\alpha(1-\upsilon_f)[1+12\ln(k)^2-6\ln(k)]$$
$$+(1-\upsilon_m)[5k^2-24\ln(k)^2-6]\}$$
$$a_1=12a^2[(1+\upsilon_m)\{k^2[4\ln(k)-3]+4\}-2\alpha\upsilon_fk^2$$
$$\times[4\ln(k)-1]+2\upsilon_m[k^2-4\ln(k)]\}]$$
$$a_2=-48(1+\alpha k^2)$$
$$C_0=48$$

a_0, a_1 and a_2 are expressions involving the material properties and geometry of the fibre–matrix system and can be evaluated for a given fibre–matrix composite.

The complete solution to Equation A10 consists of a complementary function of the form $g_1(z)=Ae^{mz}$ and a particular integral that is a constant. The four roots of m are found from the characteristic equation of the complementary function in Equation A10 and the four constants, A_1, A_2, A_3 and A_4, can be obtained by applying the boundary conditions in Equations A9 to the complete solution. The solution to Equation A10 is thus unique. In general, the roots of the characteristic equation in m may be complex.

Glossary of abbreviations and terms

L	embedded length of fibre
a	radius of fibre
b	outer radius of matrix
r,θ,z	cylindrical co-ordinate system
u	displacement in the radial direction, r
w	displacement in the axial direction, z
σ_{ij}	components of stress
ε_{ij}	components of strain
σ_{zz}	axial stress
σ^r,σ_{rr}	radial stress
$\sigma^\theta,\sigma_{\theta\theta}$	circumferential stress
σ_0	axial stress applied to fibre
ε_{zz}	axial strain
ε_{rr}	radial strain
$\varepsilon_{\theta\theta}$	circumferential strain

References

1. L. M. ZHOU, J. K. KIM and Y. W. MAI, *Comp. Sci. Technol.* **45** (1992) 153.
2. C. H. HSUEH, *Mater. Sci. Eng. A* **154** (1992) 125.
3. C. Y. YUE and W. L. CHEUNG, *J. Mater. Sci.* **27** (1992) 3173.
4. R. D. KURTZ and N. J. PAGANO, *Comp. Eng.* **1** (1991) 13.
5. C. MAROTZKE, *Comp. Sci. & Technol.* **50** (1994) 393.
6. *Idem*, *Compos. Interfaces* **1** (1993) 153.
7. J. D. WHITCOMB, R. S. RAJU and I. G. GOREE, *J. Computers & Structures* **15** (1982) 23.
8. H. C. TSAI, A. M. AROCHO and L. W. GAUSE, *Mater. Sci. Eng. A* **126** (1990) 295.
9. J. K. KIM, S. LU and Y. W. MAI, *J. Mater. Sci.* **29** (1994) 554.
10. C. L. TAN, *Private communication.*
11. T. W. CLYNE and M. C. WATSON, *Comp. Sci. Technol.* **42** (1991) 25.
12. M. Y. QUEK and C. Y. YUE, *Mater. Sci. Eng. A* **189** (1994) 105.
13. P. S. CHUA and M. R. PIGGOT, *Comp. Sci. Technol.* **22** (1985) 107.
14. C. Y. YUE and H. C. LOOI, *Composites* **26** (1995) 767.

Received 23 February 1996
and accepted 2 April 1997